International Journal of Environmental Sciences
ISSN: 2229-7359
Vol. 11 No. 23s, 2025
https://theaspd.com/index.php

Enhancing Thermal Performance of Active Magnetic Regenerator with Water-Based Nanofluid: A Simulation Study

Amrata Dwivedi[1], Aseem Chandra Tiwari[2]
[1]Mechanical engineering department, University institute of technology RGPV, Bhopal, India amrata.dwivedi10@gmail.com
[2]Mechanical engineering department, University institute of technology RGPV Bhopal, India, aseemctiwari@rgpv.ac.in

***Abstract*—*Numerical modelling was carried out to examine how dispersing copper-oxide (CuO) nanoparticles in water alters the thermal performance of active magnetic regenerator (AMR) that employs gadolinium (magnetocaloric material) as parallel plates. A two-dimensional, time-dependent COMSOL Multiphysics model simulated two working-fluid cases—pure water (0 vol %) and a 1 vol % CuO–water nanofluid—while keeping the Reynolds number and applied magnetic field identical. Thermophysical properties were obtained from empirically derived correlations in Engineering Equation Solver, reducing computational overhead. Results show that the CuO suspension widens the attainable temperature span across the AMR by roughly 0.8 K and boosts the cycle-averaged coefficient of performance (COP) by about 5 % compared with the baseline water case. The combination of an enhanced working fluid and high-conductivity copper end exchangers promotes more efficient heat exchange between the gadolinium plates and the fluid, thereby improving both temperature span and efficiency. These findings underscore the value of thermally upgraded coolants in magnetic refrigeration and demonstrate a practical simulation framework for optimizing future AMR designs.*

Keywords*—*Magneto calorific effect, Active magnetocaloric regenerator, Nanofluid, convective heat transfer, Gadolinium, COMSOL Multiphysics

I. INTRODUCTION

Magnetic refrigeration harnesses the magnetocaloric effect to move heat without relying on greenhouse gas refrigerants, making it both economical with energy and environmentally benign, Magnetic refrigeration operates on a solid-state principle, making it a sustainable and clean alternative. The performance of an active magnetic regenerator hinges on many variables, such as the magnetocaloric alloy used, the regenerator's shape and size, the cycle rate, flow speed, fluid type, and the cooling duty imposed on the system. Key performance metrics, such as the no-load temperature span, cooling capacity, and coefficient of performance (COP), are commonly used to evaluate system behaviour[1].Several studies have aimed to improve the performance of AMR systems. Ghahremani et al. (2015) [2] optimized a reciprocating AMR system by adjusting parameters such as operating frequency, fluid flow rate, and displaced volume ratio, using gadolinium as the magnetocaloric material and silicone oil as the working fluid. Their results showed up to 24% improvement in the system performance. Trevizoli et al. (2016) [3] investigated the thermodynamic characteristics of an AMR system and analysed how various operating conditions affect the temperature span, COP, and cooling output. Alahmer et al. (2021) [4] presented a comprehensive review of magnetic refrigeration technologies, reporting that AMR systems can reach up to 30–60% of Carnot efficiency while avoiding environmentally harmful refrigerants. Recently, Chdil et al. (2023) [5] incorporated artificial intelligence into AMR design and control strategies, improving predictive modelling and optimization. In another study, Scarpa, F., & Bianco, V. (2024) [6] enhanced the AMR performance using Al_2O_3-water nanofluids, where a 0.2% concentration led to a notable improvement in COP. However, higher concentrations resulted in increased pumping losses, which offset the thermal gains. Nanofluids are engineered mixtures of thermally conductive nanoparticles suspended in base fluids, have shown promise in improving heat transfer without significantly increasing viscosity. This study determines the effects of nanoparticle loading on the temperature span (ΔT), pressure drop, and overall system design, providing insights to guide the development of next-generation magnetic refrigeration systems.

II. DESCRIPTION OF MAGNETIC REFRIGERATION CYCLE

One cycle is driven by switching a magnetic field on and off and unfolds in four strokes:

- **Magnetization:** Application of magnetic field to the magnetocaloric material, causing it to heat up due to the alignment of magnetic dipoles. The fluid subsequently absorbs this heat.
- **Hot Blow:** The heated fluid carries thermal energy away from the regenerator and releases it into the HHX (hot heat exchanger), allowing heat to be transferred to the environment.
- **Demagnetization:** Removing the field disturbs the alignment, thus cools the magnetocaloric material. This creates a temperature gradient that draws heat from the fluid.
- **Cold Blow:** The cooled fluid returns to the regenerator and moves toward the CHX (cold heat exchanger), where it absorbs heat from the cooling load, thus completing the cycle.

III. MODEL DESCRIPTION

A. Geometry and Computational Domain

The AMR refrigeration system was modelled in 2D with a detailed representation of the regenerator and attached heat exchangers. Table 1 showing the Geometric configuration of the model. The regenerator consisted of an array of parallel gadolinium (Gd) plates separated by narrow channels. A total of 25 plates were included, with uniform gaps between them to form the regenerator. The working fluid oscillates through passages between the plates that span the entire regenerator, enabling efficient heat transfer. This parallel-plate configuration yielded a total regenerator stack height that contained all the plates and channels. At each end of the regenerator, a small gap of 10mm was provided in the fluid domain to connect the regenerator channels to the heat exchanger regions.

The model also includes heat exchangers HHX and CHX which are attached to the two ends of the regenerator. These blocks are positioned such that the working fluid contacts them as it exits the regenerator, thereby facilitating heat transfer. The fluid domain extended across the regenerator and included the transitional gaps to both heat exchangers. The transverse thickness of the model was considered unity and effectively modelled per unit width.

TABLE I. GEOMETRICAL CONFIGURATION OF THE MODEL.[11]

Parameter	Value	unit
Fluid channel	230x14	mm^2
CHX	50x10	mm^2
HHX	50x5	mm^2
Regenerator plates	80x0.25	mm^2
Inter plate spacing	0.3	mm

The regenerator consisted of plates fabricated from a magnetocaloric material gadolinium. The gadolinium has Curie temperature near to room temperature. In this model, the temperature and field-dependent behaviours of Gd were considered to capture the magnetocaloric effect. The adiabatic temperature change ΔTad (H, T) and specific heat Cp (H, T) of Gd under magnetic field H and temperature were considered [12], which allowed the model to accurately reproduce the response of the Gd plate to magnetization and demagnetization (heat generation/absorption due to the MCE). To accurately represent the magnetocaloric behaviour, ΔTad (H, T) and Cp (H, T) were implemented through interpolated functions fitted to data from existing study [12] for MCM, as depicted in Figures 1 The heat exchangers were made of copper, which was chosen for its high thermal conductivity and capacity to rapidly exchange heat with the fluid.

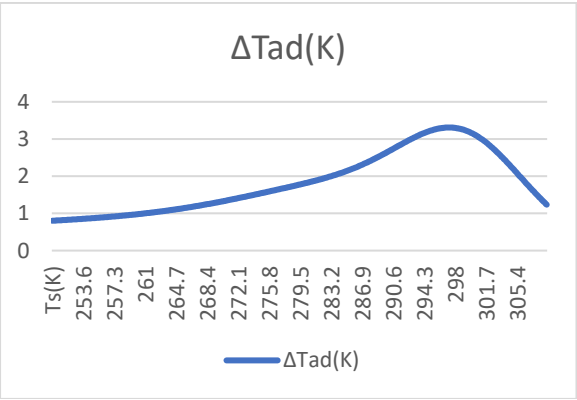

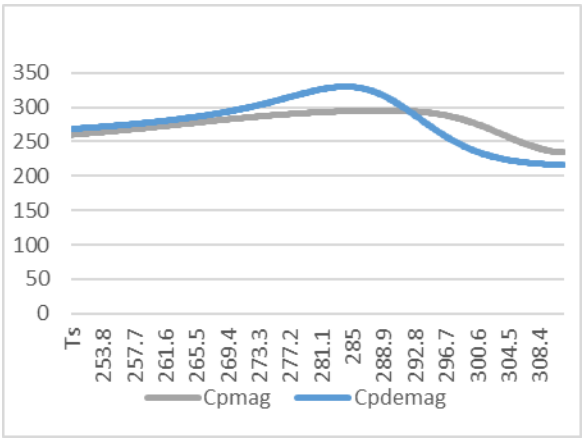

Fig. 1. ΔTad and Cp (H, T) of magnetocaloric material (gadolinium) used under a magnetic field change of 1T [12]

B. Nanofluid

TABLE II. THERMOPHYSICAL PROPERTIES OF BASE FLUID AND NANOPARTICLES. [7-9]

	Water (base fluid)	CuO (nano particle)
ρ (kg/m^3)	997	6500
μ (kg/m. s)	0.00089	~~~~
K(W/mK)	0.613	33
C_p (J/kg K)	4179	410

The essential thermophysical data for both the base water and the CuO particles summarized in Table 2 were used to derive the effective properties of the nanofluid. The thermophysical properties of nanofluids, such as density, heat capacity, thermal conductivity, and dynamic viscosity, can be described using below equations [10].

$$\frac{k_{nf}}{k_{bf}} = \frac{k_P + 2k_{bf} + 2\phi\,(k_P - k_{bf})}{k_P + 2k_{bf} - \phi\,(kp - k_{bf})} \qquad (1)$$

$$\rho_{nf} = \phi\rho_p + (1 - \emptyset)\rho_{bf} \qquad (2)$$

$$c_{Pnf} = \frac{\phi\rho_p C_{p,p} + (1 - \emptyset)\rho_{bf} c_{pbf}}{\rho_{\eta f}} \qquad (3)$$

$$\mu_{nf} = \mu_{bf}(1 + 2.5\phi + 6.2\emptyset^2) \qquad (4)$$

Where ϕ represents the nanoparticle volume fraction. Thermophysical properties of the nanofluid were calculated from nanoparticle properties and the water (base fluid) using standard mixture and suspension models, which were verified and cross-validated with data from previous studies to confirm the correctness of the measurements. To reduce the computational time associated with the COMSOL simulations, the thermophysical properties of the nanofluids (Table 3) were pre-calculated using the aforementioned equations within the Engineering Equation Solver software [10].

TABLE III. THERMOPHYSICAL PROPERTIES OF NANOFLUID

Properties	CuO-water nanofluid (1% volume fraction)
ρ (kg/m^3)	1052
μ (kg/m. s)	0.0009128
K(W/mK)	0.6306
C_p (J/kg K)	3946

C. Governing Equations and Multiphysics Coupling

A Multiphysics model was implemented to couple laminar flow dynamics with heat transfer processes occurring within both the fluid and solid regions. Unsteady incompressible flow (Navier–Stokes) and transient heat conduction/advection are the governing equations solved. The flow is assumed to be laminar (Reynolds number is low, on the order of 10 or less, owing to the small channel size and modest velocity), and the fluid is treated as incompressible. The Navier–Stokes equations consist of momentum balance and continuity. For the present model in 2D laminar, Newtonian nanofluid, the equations simplify to

$$\rho_f \left(\frac{\partial u}{\partial t} + (u \cdot \nabla)u\right) - \mu_f \nabla^2 u + \nabla p = 0 \quad (5)$$

$$\nabla u = 0 \quad (6)$$

The above equations govern the fluid velocity and pressure distribution in the fluid channels. Where ρf, μf, u, p, t are density, dynamic viscosity, velocity pressure and time respectively. A non-isothermal flow interface couples these to heat transfer equations. Solid Energy (Gadolinium and Copper): Transient heat conduction in the solid domains is modelled by

$$\rho_s C_{ps} \frac{\partial Ts}{\partial t} 2k_5 \nabla^2 T_s = \dot{Q}_{McE} + \dot{Q}_{HT} \quad (7)$$

Where Ts is the temperature of the solid, Ks is the thermal conductivity of the solid, and the source terms on the right account for any volumetric heat generation. $\dot{Q}_{McE}$ represents the heating/cooling that is magnetocaloric effect within the Gd plates, and heat transfer with the fluid is represented by$\dot{Q}_{HT}$ .Transient conduction-convection equation in the fluid is shown below

$$\rho_f c_{Pf} \left(\frac{\partial T_f}{\partial t} + (u \cdot \nabla)T_f\right) = k_f \nabla^2 T_f - \dot{Q}_{HT} \quad (8)$$

The term $(u \cdot \nabla)T_f$ accounts for convective transport of energy by the flowing nanofluid, and $k_f \nabla^2 T_f$is thermal diffusion within the fluid. Interfacial heat exchange is enforced through $\dot{Q}_{HT}$which is added to the fluid energy balance and subtracted from the solid one so that the two domains share equal and opposite heat flows. Wherever the fluid and solid are in thermal contact, the heat lost by one domain is simultaneously gained by the other, ensuring energy conservation at the interface. In practice, $\dot{Q}_{HT}$ is not an explicit source term but is handled by enforcing continuity of heat flux at fluid–solid boundaries.
This source term $\dot{Q}_{McE}$ is formulated based on the field-driven entropy change of Gd. To determine the rate of heat input We use the material's measured adiabatic temperature change ΔTad (H, T). The heat source density is defined as:

$$\dot{Q}_{McE} = \rho_{sCp(H,T)} \frac{\Delta Ta\, d(H,T)}{dt} \quad (9)$$

$\dot{Q}_{McE}$ is applied in the Gd plates (heating them by raising their entropy as if an adiabatic field increase occurred). During demagnetization (field removal), the Gd cools.

D. Boundary Conditions

Boundary conditions are applied to all external surfaces of the domain, as well as interfaces between physics are shown in Figure2.

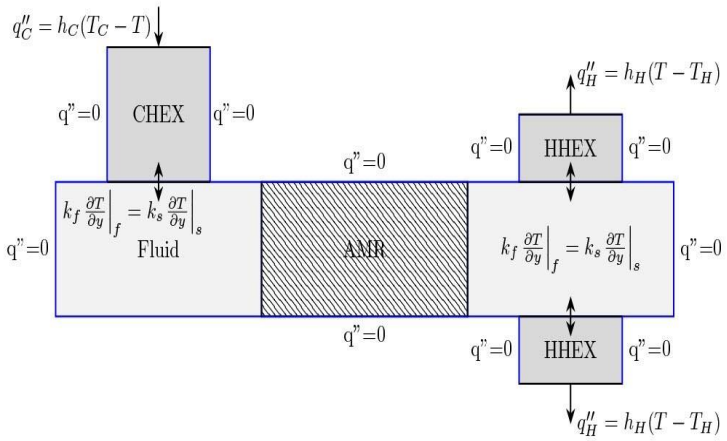

Fig. 2. Showing boundary conditions

Fluid Flow Boundaries: The fluid flow is driven in a cyclic manner to mimic the AMR Brayton cycle (cold and hot blows). Rather than a continuously open loop, the model imposes flow reversal via boundary conditions. The fluid flows from the cold end of the fluid channel toward the hot end (simulating the fluid absorbing heat from the Gd and delivering it to the hot heat exchanger) and then flow reverses from the hot end of the fluid channel to the cold end. This is implemented by prescribing a transient velocity profile at one end of the fluid channel (and an outlet or pressure condition at the opposite end), which swaps the direction every half-cycle. Specifically, a uniform inlet velocity of approximately 0.025 m/s was imposed at the inlet side during one flow half-cycle (with a corresponding outlet at the opposite side), and then the inlet/outlet roles were switched for the next half-cycle with the same speed magnitude in reverse. This yields an oscillating flow through the regenerators. All solid walls in contact with the fluid (plate surfaces and container walls) used a no-slip boundary condition. The top and bottom boundaries of the fluid domain (representing the container/channel walls above the top plate and below the bottom plate) were also treated as no-slip walls. There is no net mass flow across the system boundaries over a full cycle; the fluid oscillates back and forth inside the device.

TABLE IV. THE STARTING AND OPERATIONAL PARAMETERS OF THE MODEL.

Parameter	Value	unit
Maximum magnetic field (H_{max})	1	T
Ambient temperature	293.15	K
Total time	1800	s
Cold blow time	0.5	s
Hot blow time	0.5	s
Velocity	0.025	m/s
Magnetization step time	0.5	s
Demagnetization step time	0.5	s
CHX (h_C)	0	W/m^2K
HHX (h_H)	10E3	W/m^2K
Gadolinium initial temperature	293.15	K

Thermal Boundary Conditions: Thermal insulation (adiabatic condition) was applied to all outer boundaries of the domain, except at the external faces of the heat exchangers. The lateral sides of the regenerator (container walls along the length of the stack) and the top/bottom walls of the channel were assumed to be adiabatic (no heat loss to the environment) to focus on internal heat transfer. The external face CHX is coupled to an ambient heat sink. This was implemented by a convective heat flux condition with a convective heat transfer coefficient hc on the boundary. corresponding to a no-load condition. This allows the system to develop a maximum temperature span. Also, the external face of the hot (HHX) is coupled to an ambient heat sink. This is implemented via a convective heat flux condition on hot heat exchanger boundary, and a large heat transfer coefficient h_H is used to effectively pin the hot end to the ambient sink temperature. In physical terms, the hot exchanger is in nearly perfect thermal contact with a fluid or reservoir at ambient temperature, and continuously removes heat. The ambient temperature was

set to approximately room temperature (around the initial uniform temperature, for example, 293 K). At the fluid–solid interfaces (between the fluid and Gd plates and fluid and copper blocks), heat transfer boundary coupling is enforced: the temperature is continuous, and the heat flux is equal on both sides of the interface. In the finite element implementation, this means that the solid–fluid interface has the condition shown in figure 2. Table 4 Showing the starting and operational parameters of the model.

IV. MESH AND SOLVER SETUP

The computational domain was discretized using a normal finite-element mesh. A predominantly structured mesh (mapped quadrilateral elements) was used in the regenerator region, aligning the elements with the plate and channel geometries. The narrow 0.3 mm fluid gaps between the plates were meshed with a high density of elements across the gap. Similarly, the Gd plates and copper regions were meshed with fine elements (particularly near their surfaces) to accurately model heat conduction into and out of the fluid. A normal mesh was tested to verify that the key outputs (temperature span, etc.) changed negligibly, confirming that the chosen mesh density was sufficient. The simulation was performed as a transient time-dependent analysis to capture the cyclic operation of the AMR. A time-step of 0.5 was used for the time integration, which provided a good resolution of the flow oscillation and thermal response. The solver employs an implicit, second-order accurate backward differentiation formula (BDF) time-stepping scheme (as is the default in COMSOL for time-dependent studies). At each time step, the coupled Multiphysics equations were solved in a segregated manner. The solution process involves iteratively solving the Navier-Stokes equations to obtain updated velocity and pressure fields, which are then used to calculate the convective terms in the energy equations for both the solid and fluid. This segregated approach, under the Non-Isothermal Flow Multiphysics coupling in COMSOL, is computationally efficient and stable for conjugate heat transfer problems. The nonlinear system at each time step was solved using an iterative solver with appropriate convergence criteria (tight relative and absolute tolerances were set to ensure accurate solutions of the coupled field variables).

V. FINDINGS AND INTERPRETATION

A. Baseline Performance with Pure Water

Thermal Performance of the Baseline System: Starting from a uniform initial temperature 293 K, the system developed a significant temperature differential after 1800 sec that is 900 cycles of magnetization-demagnetization cycles. In the baseline case using pure water as the working fluid, the regenerator reached near to steady-state with 0.025 velocity and achieved temperature span of approximately 16.94 K (cold end cooling to 276.57 K while the hot end warmed to 293.51 K.

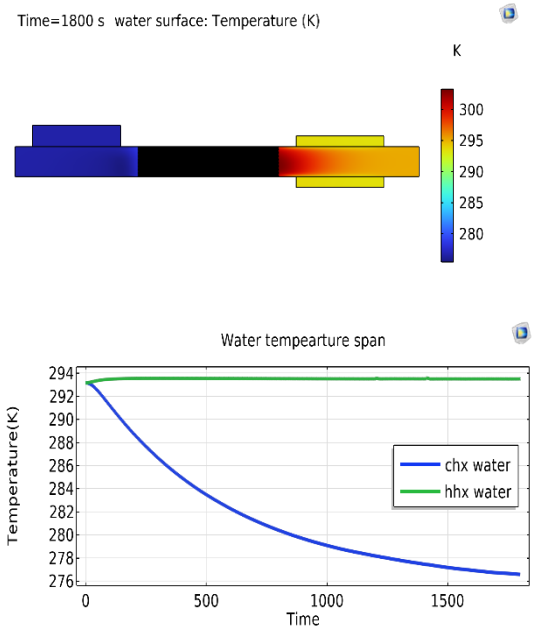

Fig. 3. Surface temperature distribution close to steady state (t ≈1800 s) and cold and hot heat exchanger temperature variation for 1800 sec for the baseline case with water

This result confirms the regenerative AMR effect, in which repeated cycles gradually increasing the temperature span. The model shows that most of the temperature drop occurs within the Gd regenerator, whereas the copper end blocks remain nearly isothermal (experiencing only a small temperature change) owing to their high thermal mass and conductivity. This design emulates ideal heat sinks and sources and is crucial for maximizing the temperature range.

B. Performance with CuO–Water Nanofluid

Replacing pure water with water-based nanofluids resulted in measurable improvements in thermal performance. Nanofluid made up of copper oxide nanoparticles had a modest increase in thermal conductivity of approximately 3% higher than that of water and a slight change in specific heat (the heat capacity of the copper oxide nanofluid was a few percent lower than that of water), and these property changes translated into improved convective heat transfer. Key performance metrics at steady state (after ~900 cycles, 1800 s of simulated time) illustrate the benefits of the nanofluid compared to pure water. Pure Water: Cold end ≈ 276.57 K; Hot end ≈ 293.51 K; Temperature span ≈ 16.94 K (baseline). CUO–Water Nanofluid: Cold end ≈ 254 K; Hot end ≈ 293.51 K; Span ≈ 17.74 K (~5% increase vs. water). Figure 4 showing the difference between the temperature span of CUO at 1% volume fraction and water.

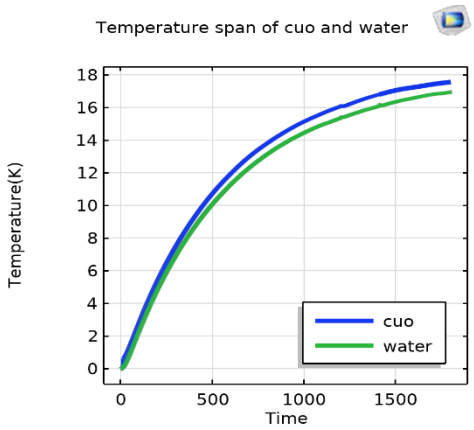

Fig. 4. Difference between the temperature span of CUO at 1% volume fraction and water ≈0.5 K

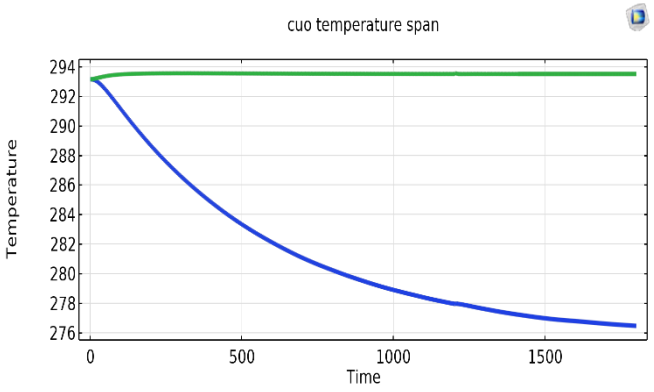

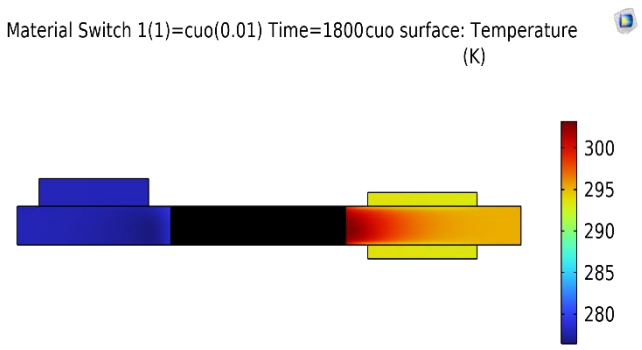

Fig. 5. Surface temperature distribution at (t ≈ 1800 s) for nanofluid CUO. and cold and hot heat exchanger temperature variation for 1800 sec for 0.1% volume CUO case.

International Journal of Environmental Sciences
ISSN: 2229-7359
Vol. 11 No. 23s, 2025
https://theaspd.com/index.php

Both cases eventually reached an almost quasi-steady cyclic regime, in which the temperature span was stabilized. The CUO nanofluid was improved the thermal conductivity (0.6306 W/m. K) and has a slightly lower specific heat than water. This implies that it cannot carry as much heat per unit mass, partly offsetting its heat transfer advantage. Consequently, compared to pure base line, the performance of the CUO nanofluid improved. The enhanced thermal performance was quantified using the integrated convective heat flux at different boundaries. The introduction of CUO nanoparticles (1%) increased the convective heat transfer rate compared to that of pure water. Specifically, the 1 vol% CUO nanofluid demonstrated an improvement in convective heat flux, reducing the maximum plate temperature swings significantly by approximately 4 K.

C. Flow Dynamics and Pressure Drop

The fluid flow remained laminar (Reynolds number on the order of a few hundred or less, given the small channel and moderate flow speed). Figure 6 confirms that the flow remains laminar

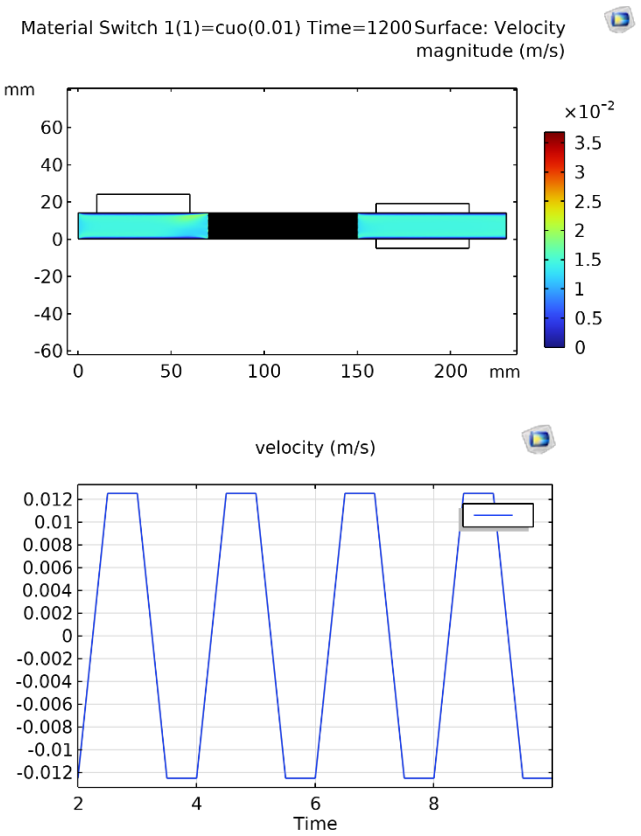

Fig. 6. Velocity magnitude field indicating laminar profile (Re < 250).

higher thermal conductivity of nanofluid decreases the thermal resistance within the fluid, enabling quicker heat transfer from the heated Gd surfaces into the fluid, during the transition from cold to hot, and from the fluid to the cooler Gd during the reverse flow from hot to cold. In essence, the temperature profile in the fluid became slightly more uniform along the flow direction when nanofluids were used, indicating more effective thermal diffusion. Furthermore, the presence of nanoparticles can induce micro-convection effects at the fluid-solid interface owing to Brownian motion (although not explicitly modelled here, the effective property approach captures some of this benefit). The slight increase in viscosity is observed in the nanofluids around 3% higher than that of water did not significantly penalize the flow or pumping power in this laminar regime; however, it could become a consideration for higher nanoparticle concentrations or turbulent flow conditions.Copper's outstanding thermal conductivity makes it an ideal material for the end heat exchangers. The cold exchanger's low thermal resistance keeps its surface temperature down, enabling it to absorb heat efficiently. On the return stroke, the high conductivity hot exchanger can quickly release stored heat into the fluid, minimizing thermal resistance in both directions of flow. Conversely, the HHX can easily transfer heat to the fluid. Our model indicates that incorporating

these conductive end sections increases the effective temperature range by providing a larger thermal reservoir. Without such heat exchangers (or with lower-conductivity materials), the ends would experience greater temperature swings, and less heat would be retained cycle-to-cycle, resulting in a smaller span.
The pressure field in Figure 7 reveals a negligible axial gradient, indicating that the ~3 % increase in nanofluid viscosity did not meaningfully increase the pumping work in this geometry.

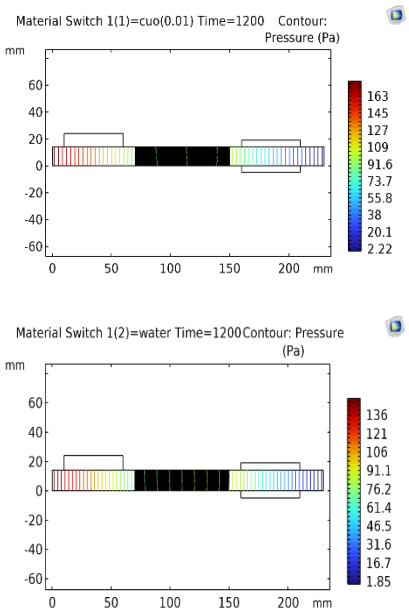

Fig. 7. Pressure distribution at (t ≈1200 s)

D. COP Evaluation Using COMSOL Outputs

To assess the efficiency of the AMR refrigeration cycle, the coefficient of performance (COP) is calculated Using COMSOL Multiphysics' built-in post-processing functions, the heat transferred at the cold and hot exchangers per cycle was obtained by integrating the thermal flux over the exchanger length and the duration of one cycle. In particular, the total heat absorbed from the cold heat exchanger (CHX) per cycle, denoted q_c', is computed as the time-integral of the heat flux $q_c''(x,t)$ along the entire length of the CHX (length L_C) over one period τ Mathematically,

$$q'_C = \int_0^{\tau} \int_0^{L_c} q''_c(x,t)\, dx\, dt$$

Likewise, the heat rejected to the hot heat exchanger (HHX) per cycle q'_H, is obtained by integrating the hot-side flux $q_H''(x,t)$ over the HHX length L_H for one cycle. These integrals were evaluated directly using COMSOL's built-in heat flux operators, which account for the normal conductive/convective heat flux through the exchanger boundaries over time.
In the absence of significant losses (e.g. negligible pressure drop and magnetic hysteresis), the magnetization work input per cycle can be inferred from the first law of thermodynamics as the difference between the heat absorbed at the cold side and the heat released at the hot side. That is, the required work per cycle for magnetization/demagnetization is taken as $w_{mag} = q_c' - q_H'$ assuming near-ideal conditions with no parasitic losses. Here w_{mag} represents the net work input to drive the magnetocaloric cycle, which in an ideal scenario equals the total work since pumping work and other losses are assumed negligible. The COP of the AMR system is then defined as the ratio of useful cooling provided to the work input.

The COP was evaluated for two different heat transfer fluids: (i) pure water and (ii) a CuO–water nanofluid at 1% volume concentration. The nanofluid yields 5% higher COP than pure water under the same operating conditions, indicating a modest performance improvement attributable to the enhanced thermal properties of the nanoparticle-laden fluid. figure 8 summarizes the COP and cooling capacity results for these cases. This trend is consistent with reports in the literature that adding high-conductivity

nanoparticles to the base fluid can improve cooling capacity and even maintain or improve COP with proper optimization

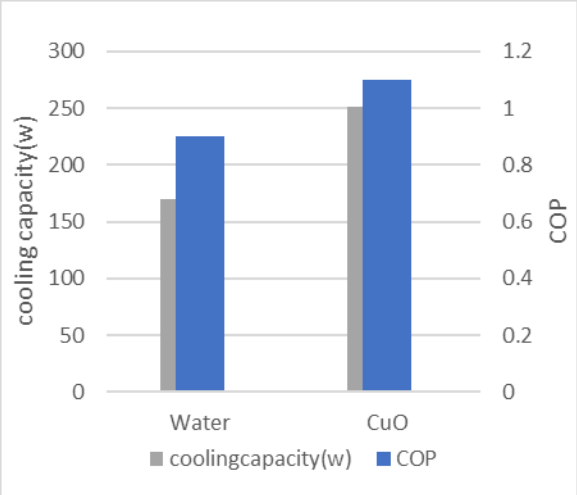

VI. CONCLUSIONS

- Incorporating nanoparticles into the base fluid notably improved its thermal conductivity, density, and viscosity, while causing a slight decrease in its specific heat capacity.
- Incorporating nanoparticles in water improved heat transfer between gadolinium plates and fluid, achieving approximately 4–5% higher temperature span compared to conventional fluids. The study's findings advocate the adoption of CUO-water nanofluids as practical coolants in AMR systems, enabling improved thermal management, extended operational cycles, and increased overall system performance.
- Integrating copper heat exchangers on either side of regenerator provided efficient thermal reservoirs, reducing thermal losses and enhancing heat flow in and out of the system.
- The results and methods presented establish a clear scientific foundation for designing high-performance AMR systems, highlighting heat transfer augmentation as crucial for achieving substantial efficiency improvements in solid-state refrigeration technologies. This numerical analysis effectively demonstrated the potential of CUO-water nanofluids for significant heat transfer enhancement in active magnetic regenerators without substantial hydrodynamic penalties Laminar flow stability was maintained with minimal (<15%) additional pressure drop, suggesting negligible additional pumping requirements.
- Initially, the system uniformly maintained at 293 K then reached almost quasi-periodic state. A periodic heating and cooling cycle occurred due to the volumetric heat source mimicking magnetization-demagnetization cycles, the nanofluid altered the heat distribution within the system, indicating a significant influence on heat transfer. CUO-water nanofluids exhibited superior heat absorption capabilities owing to their enhanced thermal properties compared to pure water. The simulation results revealed that the maximum temperature of gadolinium plates reduced by about 4 K when using a 1 vol% CUO nanofluid compared to pure water. This improvement in temperature management highlights the effectiveness of nanoparticles in enhancing heat transport capabilities.
- The introduction of a 1 vol % CuO–water nanofluid raised the cycle-averaged COP from ≈ 0.8 (pure water) to ≈ 1, corresponding to an ≈ 5 % increase in refrigeration efficiency with virtually no additional work input.

Future Work Directions in the area is to Investigate various nanofluid concentrations, nanoparticle materials, and alternative magnetocaloric alloys.

Explore realistic three-dimensional geometries and porous media structures for improved simulation accuracy and applicability.

ACKNOWLEDGMENT

The author would like to acknowledge University Institute of Technology, Bhopal (MP), India, for LAB facilities and Dr. Aseem Chandra Tiwari (HOD Mechanical Department) for valuable suggestions throughout this research work.

REFERENCES

[1] M. S. Kamran, H. O. Ahmad, and H. S. Wang, "Review on the developments of active magnetic regenerator refrigerators—Evaluated by performance," Renewable and Sustainable Energy Reviews, vol. 133, Art. no. 110247, 2020, doi: 10.1016/j.rser.2020.110247.

[2] M. Ghahremani, A. Aslani, L. H. Bennett, and E. Della Torre, "Optimization of magnetic refrigerators by tuning the heat-transfer medium and operating conditions," arXiv preprint arXiv:1511.02312, 2015.

[3] P. V. Trevizoli, A. T. Nakashima, G. F. Peixer, and J. R. Barbosa, "Performance evaluation of an active magnetic regenerator for cooling applications—Part I: Experimental analysis and thermodynamic performance," International Journal of Refrigeration, vol. 72, pp. 192–205, 2016.

[4] A. Alahmer, M. Al-Amayreh, A. O. Mostafa, M. Al-Dabbas, and H. Rezk, "Magnetic refrigeration design technologies: State of the art and general perspectives," Energies, vol. 14, no. 15, p. 4662, 2021, doi: 10.3390/en14154662.

[5] O. Chdil, M. Bikerouin, M. Balli, and O. Mounkachi, "New horizons in magnetic refrigeration using artificial intelligence," Applied Energy, vol. 335, p. 120773, 2023, doi: 10.1016/j.apenergy.2022.120773.

[6] F. Scarpa and V. Bianco, "Improving the performance of room-temperature magnetic regenerators using Al_2O_3–water nanofluid," Applied Thermal Engineering, vol. 236, Art. no. 121711, 2024, doi: 10.1016/j.applthermaleng.2023.121711.

[7] C. Popa, C. T. Nguyen, and I. Gherasim, "New specific-heat data for Al_2O_3 and CuO nanoparticles in suspension in water and ethylene glycol," International Journal of Thermal Sciences, vol. 111, pp. 108–115, 2017, doi: 10.1016/j.ijthermalsci.2016.08.016.

[8] M. A. Kedzierski, "Viscosity and density of CuO nanolubricant," Natl. Inst. Stand. Technol., Gaithersburg, MD, USA, Tech. Note, 2009.

[9] J. R. Rumble, Ed., CRC Handbook of Chemistry and Physics, 103rd ed. Boca Raton, FL, USA: CRC Press, 2022.

[10] S. K. Singh and J. S. Lee, "Performance analysis of an active magnetic regenerative system using Al_2O_3 nanofluids," International Journal of Air-Conditioning and Refrigeration, vol. 32, no. 1, p. 1450006, 2024, doi: 10.1142/S201013252450006X.

[11] F. Rodríguez-Méndez et al., "A 2D computational model of an active magnetocaloric regenerator with parallel plates," unpublished, 2023.

[12] Maiorino et al., "Evaluating magnetocaloric effect in magnetocaloric materials: A novel approach based on indirect measurements using artificial neural networks," Energies, vol. 12, no. 10, p. 1871, 2019, doi: 10.3390/en12101871.